Available online at www.sciencedirect.com

ScienceDirect

Procedia Engineering 215 (2017) 246–262

Procedia Engineering

www.elsevier.com/locate/procedia

9th International Conference on Materials for Advanced Technologies (ICMAT 2017)

PROBING PLASTICITY MECHANISMS IN LOW MELTING TEMPERATURE METALLIC NANOSTRUCTURES USING SYNCHROTRON X-RAY MICRODIFFRACTION

H. P. ANWAR ALI[1], M. KUNZ[2], N. TAMURA[2], A. S. BUDIMAN[1,*]

[1]*Xtreme Materials Lab, Pillar of Engineering Product Development, Singapore University of Technology and Design (SUTD), 8 Somapah Road, Singapore 487372, Singapore*

[2]*Advanced Light Source (ALS), Lawrence Berkeley National Laboratory, Berkeley, CA 94720, USA*

*Corresponding Author, Email: suriadi@alumni.stanford.edu , Tel: +65 64994503

Abstract

A nondestructive *ex situ* Synchrotron Laue X-ray Microdiffraction (μSLXRD) technique is used to investigate the plasticity mechanisms in the metallic nanostructures and their evolution at high homologous temperatures through analyzing low melting temperature metals such as tin. Without the use of expensive high temperature equipment, the current approach of studying plasticity mechanisms at high temperature is enabled by the low melting behaviors of the samples allowing them to provide insights on high temperature deformation mechanisms, such as thermally activated dislocation climbs. Nanopillars with a diameter near 1μm were deformed by uniaxial compression to strains of in excess of 20% at a strain rate of approximately $0.001s^{-1}$. Defect density evolution in the nanopillars was evaluated by synchrotron Laue X-ray microdiffraction (μSLXRD) before and after deformation (*ex situ*). It was found from the Laue peak broadening measurements that there was no significant change in the dislocation density of the same pillar before and after such an extent of deformation. These findings were being compared to similar experimental results of indium and gold nanopillars (from our previous reports). They were found to be in stark contrast to our previous results with indium (although both are low melting temperature metals) where the synchrotron Laue X-ray microdiffraction showed significant peak broadening – before *vs.* after the uniaxial compression to a similar amount of deformation. It appears high temperature plasticity mechanism in tin nanostructures involves significant lattice diffusion behavior, as opposed to simple displactive behavior (through dislocation movements) that has been proposed in recent studies of tin nanostructures.

Selection and/or peer-review under responsibility of the scientific committee of Symposium 2017 ICMAT.

Keywords (4-6)

tin, nanopillar, plasticity, dislocation, microstructure

1877-7058 © 2017 The Authors. Published by Elsevier Ltd.
Selection and/or peer-review under responsibility of the scientific committee of Symposium 2017 ICMAT.
10.1016/j.proeng.2017.12.146

Introduction

The “Smaller is Stronger” phenomenon [1] where crystalline materials are mechanically deformed in small volumes such as nanopillars has been ubiquitously demonstrated that the size of the sample dramatically affects the crystalline strength of materials at the micron- and nano scales. This has been revealed through uniaxial compressions over a wide range of metallic nanopillars as showcased in the reviews by Uchic *et al.* [2] and Greer and Hosson [3]. Plastic deformation in small volumes through uniaxial compression requires higher stresses than are needed for plastic flow of bulk materials. There are both extrinsic and intrinsic effects that seem to be responsible for this observation. The intrinsic effects, in contrast, are those size effects that arise in small, unconstrained single crystals under deformation. For example, indentation size effect (ISE) for crystalline materials at small depths due to geometrically necessary dislocations (GNDs) and strain gradients [4] and high strengths of sub-micron pillars of gold due to dislocation starvation hardening process [5].

Despite the fact that much has been done to evaluate the room temperature mechanical properties of metals [1–11], little experimental evidence is available to shed light on the high temperature mechanical properties of metals. Most of the work so far has been on cubic crystallographic structured metals such as gold (T_m =1085ºC), nickel (T_m =1455ºC) and molybdenum (T_m =2617ºC) where the melting temperature is way above the ambient conditions. Very few slip systems in these materials are active at room temperature (RT). To understand high temperature deformation mechanisms, one has to either use expensive equipment that works at high temperatures or find a low melting temperature metal that can behave like a high temperature material at RT.

Low melting point metals provide an advantage to gain knowledge in the high temperature plasticity/deformation mechanisms for nanostructures. In these low melting point metals, the number of active slip systems available at room temperature increases significantly with thermally activated dislocation motions such as dislocation climbs and cross slips. Nanopillars of tin (T_m =232ºC) will be studied here, and the results will be compared to similar nanopillars of indium (T_m =157ºC). Both of these metals have tetragonal structures and are much used as alternatives to lead-free solder in the microelectronic packaging industry and solar photovoltaics (PV) industries (in the thin film technology as well as the solder material in solar PV packaging industries).

There is a limited amount of experimental data at micro and nanoscales due to lack of suitable techniques that could capture the extrinsic and intrinsic behavior of materials under deformation. Synchrotron Laue X-ray Microdiffraction (μSLXRD) is a non-destructive *ex situ* technique that can be performed before and after uniaxial compression tests to understand the defect density evolution of metallic nanopillars. The dislocation defects such as statistically stored dislocations (SSD) or geometric necessary dislocations (GND) can be detected by this technique [6,12,13]. In this paper, we will talk about how the μSLXRD technique can be used to analyze and evaluate the dislocation plasticity behavior mechanisms between three materials systems – Gold [5,6,10,11,14], Indium [15–18] and Tin [12,19–22].

Through the μSLXRD technique, the dislocation behavior of gold nanopillars has been established due to dislocation source starvation effect where dislocations leave the gold crystal more frequently than they multiply, resulting in a dislocation-starved state [6]. Indium nanopillars exhibit a net increase in dislocation defect density where defect multiplication rate is greater than annihilation rate due to recovery, recrystallization and surface evaporation [16]. This behavior is similar to bulk deformation of indium.

Having many technologically important applications, such as in microelectronics as well as in solar PV packaging industries, it is important to study deformation mechanisms in tin nanostructures, particularly since recent advances in microelectronics and solar PV could lead to smaller and smaller features of tin solder. The μSLXRD technique has revealed some new insights on nanostructures of many material systems, such as gold and indium [6,16] and thus lead to further understanding of their mechanical properties in small scales that can be due to its homologous temperature, size effect and/or crystallinity of the material. Understanding and controlling plasticity and the mechanical properties of materials could thus lead to new and more robust nanomechanical structures and devices.

Experimental Methods

The Technique: Synchrotron Laue X-ray Microdiffraction

Synchrotron Laue X-ray Microdiffraction (μSLXRD) is a type of X-ray Laue diffraction technique that has been used for a variety of applications for its non-destructive nature and suitability in examining the defect structure of sub-micron and nanometer scale specimens [4,7,23–30]. The X-ray beam comes from a powerful synchrotron source, which can be focused into a submicron spot size, close to the grain size of most single crystalline materials. X-rays allow deeper penetration depths, sample preparation, and measurements under various conditions. Bragg's Law is satisfied with a white X-ray beam of a continuous range of wavelengths, allowing a huge number of reflections to be obtained simultaneously even when the lattice is locally rotated or bent, resulting in the observation of streaked Laue spots. Laue diffraction also enables the exploration of the point defects, coherent precipitates, dislocations, stacking faults or grain boundaries in defect structure of imperfect crystals. Thus, the polychromatic characteristic of the synchrotron radiation makes it sensitive to local lattice curvature or rotation in the crystals under consideration. It is this sensitivity to local lattice curvatures that makes the μSLXRD technique is suitable for probing plasticity at small scales since strain gradients and geometrically necessary dislocations (GNDs) are directly related to the local lattice curvatures [6,12,13].

This technique involves scanning the sample with the focused X-ray beam at submicron resolution, thus gaining structural information about the crystal and its defects in the diffracted volume through the shapes of the Laue diffraction peaks. Using this approach, we can monitor the change in the Laue diffraction peaks before and after deformation. A quantitative analysis of the Laue peak widths then allows us to estimate the density of GNDs in the sample. The absolute number of GNDs in the crystal can be determined using the relevant dimensions of the sample. A comparison of the numbers of GNDs before and after, or even during, the deformation provides information about the change in microstructure associated with plastic deformation. Conventional structural characterization methods such as transmission electron microscope (TEM) [31] and Resonant Ultrasound Spectroscopy (RUS) [32,33] will expose the structure to high energy electron beams and sounds that might alter the internal defect structure during analysis.

The microstructure of as-fabricated and uniaxially compressed nanopillars was characterized by the μSLXRD technique with Beamline 12.3.2 at the Advanced Light Source synchrotron facility at Lawrence Berkeley National Laboratory, Berkeley, CA [29,34] as shown in Figure 1. Only tin nanopillars with a diameter of 920nm were characterized as diffracted X-ray signals from smaller diameter pillars were not reliable. The energetic X-rays are not damaging to the internal nanopillar structure since there is negligible change in the sample temperature during measurements, making the μSLXRD technique especially useful for low melting temperature metals.

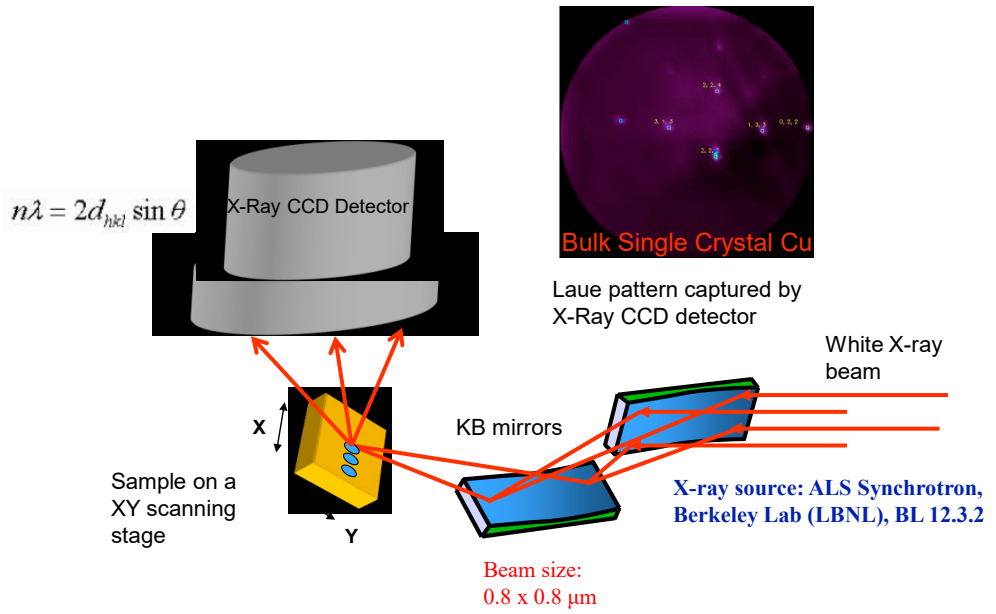

Fig. 1: Schematic Layout of the Beamline (BL) 12.3.2 at the Advanced Light Source (ALS)

Each nanopillar sample was mounted on a MICOS high precision XY-positioning stage (resolution of 0.05μm) and raster scanned under the white X-ray beam with the purpose of locating the nanostructures. This imaging process provided both X-ray microfluorescence (μXRF) and the X-ray microdiffraction information of the scanned area. The μSLXRD patterns were collected using a MAR 133 X-ray charge coupled device (CCD) detector with pixel size near 100μm and analyzed using a custom-made XMAS software package [13].

Previous work by Budiman *et al.* [8] has detailed the steps for the μXRF followed by the μSLXRD scanning of the nanopillar [6]. The chosen X-ray scan area of an individual nanopillar is a ~10x10μm^2 square with 0.5μm step sizes. The μSLXRD scan process involved the collection of 400 CCD frames, which required 3-4h to collect. The exposure time for each frame was 5s, in addition to about 10s of electronic readout time.

With μSLXRD, the change in the Laue diffraction images before and after uniaxial compression of nanopillars can be monitored. A quantitative analysis of the Laue peak widths allows us to estimate the density of GNDs in the submicron pillars from the Cahn-Nye relationship of the local GND density is $\rho = |\kappa|/b$ where κ is the local curvature and b is the magnitude of Burger's vector [35,36]. The absolute number of dislocations in the single crystal can be derived with the exact geometries of the pillars, $n = \rho WH = WH|\kappa|/b$, where W and H are diameter and height of the pillar [6]. A comparison of the number of dislocations before and after the uniaxial compression would unveil the change in the material involved in the deformation.

Fabrication of Nanopillars

The tin nanopillars were made by the electron beam lithography followed by metal electroplating (EBL&ME). The EBL&ME method was developed by Burek and Greer first for gold [14] and tin nanopillars [19]. The specific procedure to generate indium nanopillars is described in [17]. The fabrication of the samples was done in collaboration with Dr. D. Jang (of KAIST), Dr. M. Burek (of Harvard University) and Prof. T. Tsui (of University of Waterloo) [14,16–19]. This method allows for large number of varying-sized nanopillars over a short period of time. Seed layers of titanium (20nm) and gold (100nm) are deposited by electron beam evaporation before lithography of PMMA beams to act as a cathode in subsequent electroplating steps, encouraging the growth of the nanopillars during electroplating. The resulting nanopillar diameters are of a wide range of between ~70-920nm with aspect ratios of 2-4 and separation distance of 10μm. Figures 2 and 3 show the SEM micrographs of an array of 920nm diameter tin pillars. A 15-day rest period was maintained for all nanopillar samples prior to microstructural and mechanical characterization to ensure thermally activated processes such as grain growth or annihilation of fabrication induced defects at free surfaces had reached equilibrium at RT prior to testing.

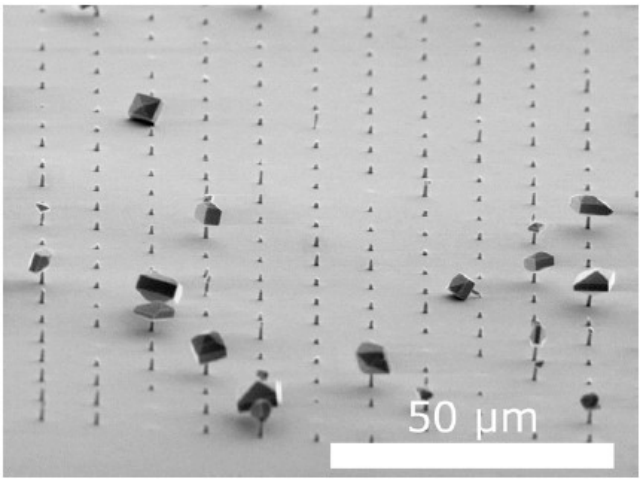

Fig. 2. An array of 920 nm diameter tin pillars in a 100 x 100 µm array. Reprinted with permission from [19]

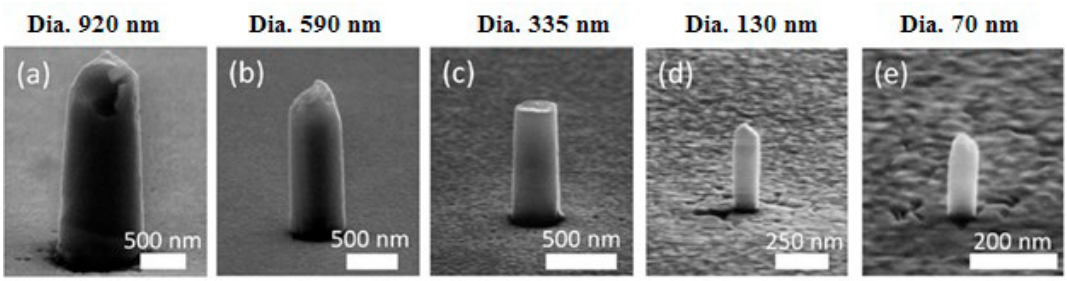

Fig. 3: Tin nanopillars fabricated with various diameters from 200 to 920 nm. Reprinted with permission from [19]

Ex-situ Uniaxial Compression Tests

The uniaxial compression tests were conducted at Stanford University using the same tool of the Nanoindenter XP (Agilent/MTS, Knoxville, TN) with a custom flat punch diamond tip. The compression tests were done by displacement control in continuous stiffness mode (CSM) of the instrument. The strain rates used in the tests were mainly $0.001s^{-1}$ with additional studies at $0.01s^{-1}$ and $0.0001s^{-1}$. The data obtained during compression were then converted to uniaxial stresses and strains using the assumption that the plastic volume is conserved throughout this mostly homogeneous deformation. For indium and tin, the deformed nanopillars were stored in the dry ice sublimation environment (-78.5ºC) during transportation for the synchrotron experiments to prevent additional dislocation activities due to temperature.

Results and Discussion

Ex-situ Uniaxial Compression Tests

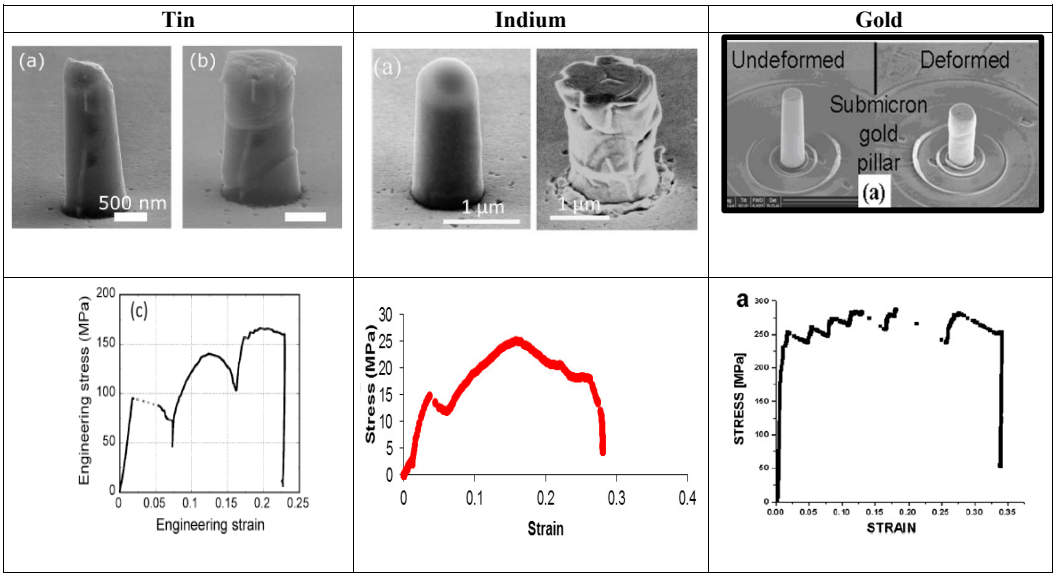

Fig. 4: SEM micrographs of tin, indium and gold nanopillars (a) before and (b) after uniaxial compression and (c) their respective engineering Stress-strain graphs. Reprinted with permission from [19] for Tin, [16] for Indium and [6] for Gold

The engineering stress-strain curves of tin, indium, and gold were obtained under displacement control of uniaxial compression with a strain rate of 0.001 s^{-1} as shown in Figure 4. From tin's engineering stress-strain curve, the nanopillar exhibits strain bursts after the initial yielding. The max flow stress (measured as 5% strain) observed is 80MPa. This is known to be due to the sudden shear failures along the crystallographic slip planes. Crystallographic shear offsets, sidewall surface wrinkles and bulges perpendicular to the loading direction are observed on its post compressed pillars while trying to maintain its shape.

However, the engineering stress-strain curve of similar tetragonal indium reveals that this sample was quite soft with a flow stress (measured at 5% strain) of ~13MPa. Post SEM image of indium provides no evidence of the plastic strain being carried out by significant crystallographic shear offsets but instead accommodated by sidewall wrinkling, bulging and folding. There are no discrete slip bands observed in this deformed sample.

For FCC gold, the uniaxial loading in the <111> direction of the nanopillar saw its initial flow stress reaching 250MPa at 2% engineering strain. It reached the maximum yield strength of 280MPa, close to 10 times the yield stress of gold in bulk. It observed multiple strain bursts after the initial yielding too. The post-compressed gold pillar remains centrally loaded and preserves its cylindrical shape throughout the deformation process. Visible slip markings were observed on the deformed surface of the pillar that appears to be along {111} plane.

µSLXRD Laue Diffraction Peak Profile Comparison

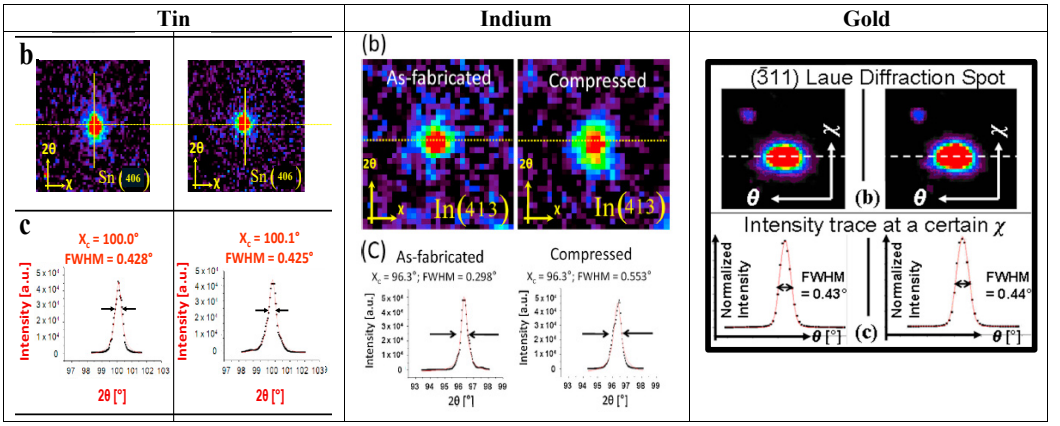

Fig. 5: µSLXRD Laue diffraction pattern and their intensity plot comparisons between tin, indium and gold nanopillars (a) before and (b) after uniaxial compression. The diffraction spots have been converted to reciprocal q space. Reprinted with permission from [16] for Indium and [6] for Gold

For the three materials, a single unique Laue diffraction pattern (not shown here) belonging to a (204) body-centered tetragonal (BCT) crystal for tin, a (111) face-centered tetragonal (FCT) crystal for indium and a (111) face-centric cubic (FCC) crystal for gold was identified for the entire nanopillar volume. These specimens consist of a very large grain which occupies the majority of the nanopillar volume, and any remaining grains are too small to diffract enough incident X-ray signals for detection.

Both pre- and post Laue diffraction spots for all three materials, tin, indium, and gold have the same shape and that they are both rounded – not broadened towards a certain direction as shown in Figure 5. This rounded shape is typical of an undeformed crystal whereas broadening of a Laue diffraction spot in a certain direction (streaking) would have been associated with the presence of strain gradients in the deformation volume. The crystals in the nanopillars were well annealed with no excess initial dislocations of the same size (i.e. no GNDs).

Further, no crystal rotation was observed up to the maximum compressive strain performed in the experiment. The intensity traces are taken along a particular χ angle to study the Laue diffraction peak profile more quantitatively. The χ angle defined in the plot is orthogonal to 2θ. The profiles were fitted with Lorentzian curves. This peak broadening consists of three contributions: crystal size effect, instrumentation and the possibility of random dislocation storage during fabrication.

The intensity trace of tin Sn (406) Laue diffraction peaks taken from uniaxially compressed tin nanopillars demonstrated negligible peak broadening relative to their as-fabricated state. The measured FWHMs of both tin (406) Laue spots profiles show that there is a decrease of 0.03° in the angular width. This is similarly observed in gold where their difference in measured FWHMs of both gold (-3 11) Laue spots profiles showed an increase of 0.01° in the angular width. Both of these differences are still within the experimental error bar of instrumentation [37,38], rendering the pre- and post- uniaxial compression measurements statistically identical.

However, the size of Indium (413) post-compression Laue diffraction spots are significantly larger than those from the as-fabricated state. The amount of diffraction peak broadening is quite different between the as-fabricated and post-compression results as the peaks have the full-width-half-max (FWHM) values of 0.298° and 0.553° respectively. This increase of peak width by 0.255° is likely a result of defect accumulation, implying that the rate of defect generation during deformation exceeded that of annihilation, where some of these defects can be dislocations. There is also a lack of crystal rotation even after near 28% compressive strain. This is another indicator that a large number of active systems were available during indium nanopillar compression to avoid rotational deformation.

Discussion

It appears from the uniaxial compression engineering stress-strain curves as well as the μSLXRD Laue diffraction results that BCT tin seems to behave closer to that of FCC gold compared to that of FCT Indium. A recent experiment by Philippi *et al.* considered tin micropillars of diameters between 1 to 10μm and performed ex-situ μSLXRD experiments to determine the effect of size and orientation behavior of tin micropillars on its mechanical behavior [12]. Irrespective of the slip plane orientation it was compressed (*i.e.* [001] and [110] directions), their Laue data observed a negligible amount of peak broadening with less than 10 geometrically

necessary dislocations (GNDs) at the sample center. This is similar to our μSLXRD result based on the calculation using the Cahn-Nye relation of $\boldsymbol{\rho} = \frac{|\boldsymbol{\kappa}|}{\boldsymbol{b}}$ [35,36] to determine the number of dislocations left in the crystal of the whole width of pillar to be 7-8 dislocations. In comparison, the number of dislocations left in the crystal for gold was found to be 3-4 dislocations [6] and indium can be approximated to 15 dislocations. Burek *et al.* justified this with their initial synchrotron μSLXRD findings of tin nanopillars that was done in collaboration with our group [19] that since there is no significant peak broadening between the pre and post compression data, it can be assumed to be behavior follow mechanisms similar to that of gold. However, our subsequent analysis appears to suggest other mechanisms might be in play in the case of tin nanostructures (compared to that of gold nanostructures) exactly due to its low melting temperature property.

Gold is a face-centred cubic (FCC) crystal with a melting temperature of 1064ºC. This, in turn, results in a homologous temperature of 0.1 for experiments done at room temperature (RT). Like typical FCC metal at room temperature, there are only a limited set of active systems for dislocation glide. Dislocation motion is often constrained to a specific slip system, whereby dislocations glide along the crystal planes with the lowest critical resolved shear stress (CRSS) until they reach the free surface, shearing the crystal along that crystallographic plane. The compression behavior observed by gold nanopillars is explained by the dislocation starvation effect [5,10] where the rate at which the mobile defects annihilate at the sample surfaces is far greater than the rate at which defects generate or multiply. The total distance that a dislocation travels before reaching a free surface is essentially a straight line.

However, the dislocation behavior at room temperature for low temperature metals such as indium and tin would also involve thermally activated processes such as cross slip and dislocation climb. These processes are expected to have a non-trivial contribution in the mechanical deformation of these structures and might even be annihilated.

Indium is a face centered tetragonal (FCT) and space group of I 4 / mmm. At room temperature, indium undergoes recovery and recrystallization due to its low melting point of 157ºC which results in a homologous temperature of ~0.7. Budiman *et al.* quantified the net increase of defect density seen from Laue peak

broadening of indium is due to the competition between defect multiplication rate from the dislocation-dislocation interactions and generation of dislocation sources and annihilation from the thermally activated processes [16]. The symmetrical broadening of the rounded peak is taken to be an accumulation of asymmetric broadening peaks activated simultaneously in multiple directions.

Tin is a body centered tetragonal (BCT) with c/a = 0.5456 and space group of I 4 1/amd. It has a melting temperature of 232ºC or (505K) which results in a homologous temperature of ~0.6. At room temperature, tin exists as a β-allotrope (white tin), and three of the most commonly observed BCT tin slip systems are (110)[-111], (110)[001] and (100)[010] [39]. It seems expected that the dislocation behavior should be close to indium based on its crystallographic tetragonal character. This is observed for most FCC and BCC metal trends [3].

Besides crystallographic character, another factor is the size effect between the three materials. For nanopillars, size effect in strength is frequently described with power law equation of $\sigma \sim d^{-m}$, where d is the size or the diameter and m is the size exponent . Burek *et al.* compressed different diameter sizes of tin nanopillars (350nm, 560nm and 920nm) at a constant strain rate of ~0.001s^{-1} and plotted the engineering flow stress measured at 5% flow stress as function of feature size and found that slope of the log-log plot to be ~0.572 [19]. Recently, Kim *et al.* summarized Burek's results with their own results for 1µm and 5µm nanopillars and concluded with the exponent of ~0.70 [20] and Philippi *et al.* observed the exponent of ~1 [12]. However, as the diameter is reduced from 450nm to 130nm, Tian *et al.* observed a different kind of size behavior at same 0.001s^{-1} compared to the faster strain rate of 0.01s^{-1} where diffusional deformation through coble creep replaces the displactive plasticity as the dominant deformation mechanism at room temperature [22]. In some sense, there is some size effect experienced in tin depending on the diameter size of nanopillar being considered. In comparison, FCC gold observes a strong size effect with the size effect of ~0.66 [10]. This is in line with typical values for FCC metals [3]. Indium didn't observe a clear size effect trend with the different size diameter nanopillars for the same 0.001s^{-1} strain rate [18].

It is thus observed that 920nm diameter tin nanopillars experience the size effect phenomenon closer to FCC gold rather than following close to indium which exemplifies typical low melting temperature behavior at room

temperature. A cause for this can be seen from the constant temperature with varying stress level creep experiments within the elastic regime performed by Kim *et al.* on 1µm and 5µm diameter single crystal pillars [20]. From their experiments, they observed huge creep deformation at room temperature and creep stress exponent close to 1 which indicates atomic diffusion governs the overall creep process. This is unlike bulk Sn which observes dislocation climb with a typical stress exponent of ~3-7 and creep activation energy close to atomic self-diffusion [40,41]. Further evaluation with in-situ SEM creep tests confirmed it was due to lattice diffusion rather than coble creep that resulted in the behavior of the tin nanopillars. However, for indium nanopillars, Lee *et al.* observed creep stress exponent be approximately 6 regardless of the size of pillars observed. This suggests a dislocation nucleation dominated bulk-scale mechanism [18]. No comparative work could be found for gold nanopillars of similar grain size.

This explains the behavior why the examined 920nm diameter tin nanopillars observed no change in the Laue peak broadening post compression. Though tin has multiple slip systems and has a relatively high homologous temperature, the preferred path for dislocations seems to change with the grain size of the metal. As shown by Kim *et al.* [20], the dislocations in 920nm tin nanopillars prefer to move by atomic diffusion changes to the lattice in nanopillars in comparison to bulk-like deformation behavior in indium shown by Lee *et al.* [18] and Budiman *et al.* [16].

It is through its size effect from bulk to the nanoscale regime that enables it to transition from the typical power law creep behavior to a diffusion flow based behavior. An interesting future work would be to understand the evolution of defect densities of metals with established size effect behavior of different diameter size nanopillars for comparison with our present work.

Conclusion

The use of Synchrotron Laue x-ray microdiffraction (μSLXRD) as a technique for probing high temperature deformation mechanisms is showcased here with the evolution of defect densities comparison of two low melting temperature tetragonal metals of tin and indium together with the establish gold nanopillars. The μSLXRD technique clearly identified tin to be similar to gold in terms of negligible dislocations with no significant increase in the Laue diffraction peak widths. The size effect of the tin nanopillars causes the transition in dislocation behavior from dislocation nucleation mechanisms to lattice diffusion based one. Thus, it is not sufficient to just look at the low melting temperature metals but also the size dimension at which it is to be studied to understand the high temperature mechanisms in metals.

Acknowledgements

The authors acknowledge M. Burek (of Harvard University), D. Jang (of KAIST) and T. Tsui (of University of Waterloo) for the fabrication of the tin nanopillars. The authors also acknowledge the interesting discussions with Prof. William D. Nix (of Stanford University) about the plasticity of metallic nanostructures in confined volumes. The new addition of tin synchrotron data work was supported by the Office of Science, Office of Basic Energy Sciences, of the US Department of Energy. The Advanced Light Source was supported by the Director, Office of Science, Office of Basic Energy Sciences, Materials Sciences Division of the U.S. Department of Energy under Contract No. DE-AC02-05CH11231 at Lawrence Berkeley National Laboratory and the University of California, Berkeley, California. One of the authors (ASB) was supported by the Director, Los Alamos National Laboratory (LANL), under the Director's Postdoctoral Research Fellowship program (#20090513PRD2). The authors would like to thank the critical support and infrastructure provided by Singapore University of Technology and Design (SUTD) during the manuscript preparation is highly appreciated. The authors also gratefully acknowledge the funding and support from SUTD-MIT International Design Centre (IDC), Singapore for the project under IDC Grant, IDG31400102.

References

[1] M.D. Uchic, D.M. Dimiduk, J.N. Florando, W.D. Nix, Sample dimensions influence strength and crystal plasticity, Science. 305 (2004) 986–989.

[2] M.D. Uchic, P.A. Shade, D.M. Dimiduk, Plasticity of micrometer-scale single crystals in compression, Annual Review of Materials Research. 39 (2009) 361–386.

[3] J.R. Greer, J.T.M. De Hosson, Plasticity in small-sized metallic systems: Intrinsic versus extrinsic size effect, Progress in Materials Science. 56 (2011) 654–724.

[4] G. Feng, A. Budiman, W. Nix, N. Tamura, J. Patel, Indentation size effects in single crystal copper as revealed by synchrotron x-ray microdiffraction, Journal of Applied Physics. 104 (2008) 043501.

[5] J.R. Greer, W.C. Oliver, W.D. Nix, Size dependence of mechanical properties of gold at the micron scale in the absence of strain gradients, Acta Materialia. 53 (2005) 1821–1830.

[6] A. Budiman, S. Han, J. Greer, N. Tamura, J. Patel, W. Nix, A search for evidence of strain gradient hardening in Au submicron pillars under uniaxial compression using synchrotron X-ray microdiffraction, Acta Materialia. 56 (2008) 602–608.

[7] A. Budiman, W. Nix, N. Tamura, B. Valek, K. Gadre, J. Maiz, et al., Crystal plasticity in Cu damascene interconnect lines undergoing electromigration as revealed by synchrotron x-ray microdiffraction, Applied Physics Letters. 88 (2006) 233515.

[8] U. Chakkingal, A.B. Suriadi, P. Thomson, The development of microstructure and the influence of processing route during equal channel angular drawing of pure aluminum, Materials Science and Engineering: A. 266 (1999) 241–249.

[9] U. Chakkingal, A.B. Suriadi, P. Thomson, Microstructure development during equal channel angular drawing of Al at room temperature, Scripta Materialia. 39 (1998) 677–684.

[10] J.R. Greer, W.D. Nix, Nanoscale gold pillars strengthened through dislocation starvation, Physical Review B. 73 (2006) 245410.

[11] S.-W. Lee, S.M. Han, W.D. Nix, Uniaxial compression of fcc Au nanopillars on an MgO substrate: The effects of prestraining and annealing, Acta Materialia. 57 (2009) 4404–4415.

[12] B. Philippi, C. Kirchlechner, J.S. Micha, G. Dehm, Size and orientation dependent mechanical behavior of body-centered tetragonal Sn at 0.6 of the melting temperature, Acta Materialia. 115 (2016) 76–82.

[13] N. Tamura, XMAS: a versatile tool for analyzing synchrotron X-ray microdiffraction data, Strain and Dislocation Gradients from Diffraction. Spatially Resolved Local Structure and Defects. (2014) 125–155.

[14] M.J. Burek, J.R. Greer, Fabrication and microstructure control of nanoscale mechanical testing specimens via electron beam lithography and electroplating, Nano Letters. 10 (2009) 69–76.

[15] G. Feng, A. Ngan, Creep and strain burst in indium and aluminium during nanoindentation, Scripta Materialia. 45 (2001) 971–976.

[16] A.S. Budiman, G. Lee, M.J. Burek, D. Jang, S.M.J. Han, N. Tamura, et al., Plasticity of indium nanostructures as revealed by synchrotron X-ray microdiffraction, Materials Science and Engineering: A. 538 (2012) 89–97.

[17] G. Lee, J.-Y. Kim, A.S. Budiman, N. Tamura, M. Kunz, K. Chen, et al., Fabrication, structure and mechanical properties of indium nanopillars, Acta Materialia. 58 (2010) 1361–1368.

[18] G. Lee, J.-Y. Kim, M.J. Burek, J.R. Greer, T.Y. Tsui, Plastic deformation of indium nanostructures, Materials Science and Engineering: A. 528 (2011) 6112–6120.

[19] M.J. Burek, A.S. Budiman, Z. Jahed, N. Tamura, M. Kunz, S. Jin, et al., Fabrication, microstructure, and mechanical properties of tin nanostructures, Materials Science and Engineering: A. 528 (2011) 5822–5832.

[20] Y.-J. Kim, N. Qaiser, S.M. Han, Time-dependent deformation of Sn micropillars, Materials \& Design. 102 (2016) 168–173.

[21] A. Lupinacci, J. Kacher, A. Eilenberg, A. Shapiro, P. Hosemann, A. Minor, Cryogenic in situ microcompression testing of Sn, Acta Materialia. 78 (2014) 56–64.

[22] L. Tian, J. Li, J. Sun, E. Ma, Z.-W. Shan, Visualizing size-dependent deformation mechanism transition in Sn, Scientific Reports. 3 (2013) 2113.

[23] A.S. Budiman, Probing crystal plasticity at the nanoscales: Synchrotron X-ray microdiffraction, Springer, 2015.

[24] A. Budiman, K.R. Narayanan, N. Li, J. Wang, N. Tamura, M. Kunz, et al., Plasticity evolution in nanoscale Cu/Nb single-crystal multilayers as revealed by synchrotron X-ray microdiffraction, Materials Science and Engineering: A. 635 (2015) 6–12.

[25] A. Budiman, H.-A.-S. Shin, B.-J. Kim, S.-H. Hwang, H.-Y. Son, M.-S. Suh, et al., Measurement of stresses in Cu and Si around through-silicon via by synchrotron X-ray microdiffraction for 3-dimensional integrated circuits, Microelectronics Reliability. 52 (2012) 530–533.

[26] V. Handara, I. Radchenko, S. Tippabhotla, K.R. Narayanan, G. Illya, M. Kunz, et al., Probing stress and fracture mechanism in encapsulated thin silicon solar cells by synchrotron X-ray microdiffraction, Solar Energy Materials and Solar Cells. 162 (2017) 30–40.

[27] C.Y. Khoo, H. Liu, W.A. Sasangka, R.I. Made, N. Tamura, M. Kunz, et al., Impact of deposition conditions on the crystallization kinetics of amorphous GeTe films, Journal of Materials Science. 51 (2016) 1864–1872.

[28] I. Radchenko, S. Tippabhotla, N. Tamura, A. Budiman, Probing phase transformations and microstructural evolutions at the small scales: synchrotron X-ray microdiffraction for advanced applications in 3D IC (integrated circuits) and solar PV (photovoltaic) devices, Journal of Electronic Materials. 45 (2016) 6222–6232.

[29] N. Tamura, R. Celestre, A. MacDowell, H. Padmore, R. Spolenak, B. Valek, et al., Submicron x-ray diffraction and its applications to problems in materials and environmental science, Review of Scientific Instruments. 73 (2002) 1369–1372.

[30] S.K. Tippabhotla, I. Radchenko, W. Song, G. Illya, V. Handara, M. Kunz, et al., From cells to laminate: probing and modeling residual stress evolution in thin silicon photovoltaic modules using synchrotron X-ray micro-diffraction experiments and finite element simulations, Progress in Photovoltaics: Research and Applications. 25 (2017) 791–809.

[31] S. Yamada, T. Sakai, In situ transmission electron microscopy observation of dislocation motion in 9Cr steel at elevated temperatures: influence of shear stress on dislocation behavior, Microscopy. 63 (2014) 449–461.

[32] F. Barra, A. Caru, M.T. Cerda, R. Espinoza, A. Jara, F. Lund, et al., Measuring dislocation density in aluminum with resonant ultrasound spectroscopy, International Journal of Bifurcation and Chaos. 19 (2009) 3561–3565.

[33] F. Barra, R. Espinoza-González, H. Fernández, F. Lund, A. Maurel, V. Pagneux, The use of ultrasound to measure dislocation density, JOM. 67 (2015) 1856–1863.

[34] M. Kunz, N. Tamura, K. Chen, A.A. MacDowell, R.S. Celestre, M.M. Church, et al., A dedicated superbend X-ray microdiffraction beamline for materials, geo-, and environmental sciences at the

advanced light source, Review of Scientific Instruments. 80 (2009) 035108.

[35] R. Cahn, Recrystallization of single crystals after plastic bending, Journal of the Institute of Metals. 76 (1949) 121.

[36] J. Nye, Some geometrical relations in dislocated crystals, Acta Metallurgica. 1 (1953) 153–162.

[37] A. MacDowell, R. Celestre, N. Tamura, R. Spolenak, B. Valek, W. Brown, et al., Submicron X-ray diffraction, Nuclear Instruments and Methods in Physics Research Section A: Accelerators, Spectrometers, Detectors and Associated Equipment. 467 (2001) 936–943.

[38] N. Tamura, A. MacDowell, R. Spolenak, B. Valek, J. Bravman, W. Brown, et al., Scanning X-ray microdiffraction with submicrometer white beam for strain/stress and orientation mapping in thin films, Journal of Synchrotron Radiation. 10 (2003) 137–143.

[39] F. Yang, J. Li, Deformation behavior of tin and some tin alloys, Journal of Materials Science: Materials in Electronics. 18 (2007) 191–210.

[40] M. Mathew, H. Yang, S. Movva, K. Murty, Creep deformation characteristics of tin and tin-based electronic solder alloys, Metallurgical and Materials Transactions A. 36 (2005) 99–105.

[41] G. Zhao, F. Yang, Effect of DC current on tensile creep of pure tin, Materials Science and Engineering: A. 591 (2014) 97–104.